IEEE Access
Multidisciplinary ⋮ Rapid Review ⋮ Open Access Journal

Received 9 May 2023, accepted 19 May 2023, date of publication 24 May 2023, date of current version 14 June 2023.

*Digital Object Identifier 10.1109/ACCESS.2023.3279496*

RESEARCH ARTICLE

# WOMT: Wasserstein Distribution Based Minimization of False Positives in Breast Tumor Classification Using Deep Learning

**L. LAKSHMI[1], KUNADA DHANA SREE DEVI[2], SHIKHA GUPTA[3], K. ADI NARAYANA REDDY[1], SURESH KUMAR GRANDHI[4], AND SANDEEP KUMAR PANDA[1], (Member, IEEE)**

[1]Department of Artificial Intelligence and Data Science, Faculty of Science and Technology (IcfaiTech), ICFAI Foundation for Higher Education (IFHE), Hyderabad 501203, India
[2]Department of Computer Science and Engineering, Gitam University, Hyderabad, Telangana 502329, India
[3]Department of Computer Science and Engineering, Chandigarh University, Punjab 140413, India
[4]Department of Mechanical Engineering, Faculty of Science and Technology, ICFAI Foundation for Higher Education (IFHE), Hyderabad 501203, India

Corresponding author: Sandeep Kumar Panda (sandeeppanda@ifheindia.org)

This work was supported by the ICFAI Foundation for Higher Education, Hyderabad, Telangana, India.

**ABSTRACT** Women's life suffered and killed by invasive cancerous tumors is the most frequently highlighted header in many newsletters since 2010. There can be many. By their nature, invasive tumors spread from tissue to tissue and abduct themselves to cause new tumors. In many of the human biological parts, CT scan has given an objective approach to the early and successful detection of cancerous tumors. However, there were cases where diagnosis with CT scan images failed, resulting in many false positives. In economically backward countries, these false positives raised the notifying concern of women who cannot afford multiple diagnostic tests. Due to changes in biological metabolism, the growth of breast fat in women to considerably abnormal size is the main cause of false positives. In many of the images under study, this huge thick breast fat layer led to the rise of misclassification rate with false positives. Rendering societal help requires a precise mechanism that can reduce the false positives at an initial diagnosis. The proposed method introduces a novel constraint-based algorithm to classify a mammogram image as cancerous, aiming to reduce false positives. The proposed deep learning algorithm WOMT is trained with Wasserstein Distribution constraints that are derived from the mass transfer of cancerous patches to non-cancerous patches. The experimental simulations with a deep learning model trained with these constraints resulted in reduced false positives.

**INDEX TERMS** Bhattacharya's similarity, CNN, false positives, optimal mass transfer, Wasserstein distribution.

## I. INTRODUCTION

Between 10-15 % of women worldwide, who are within the age groups of 30 and above, are affected by invasive breast cancer. As the most diagnosed cancer in many American-Euro countries, its crude increasing incidence rate is causing researchers to focus on developing tools and methods for early detection. This focus is more on cancer detection with the advent of more sophisticated AI and ML Technology [1]. Studies show that this cancer has varied in women's mortality in most economically backward countries. The factors for this mortality and incidence variations as studied are availability, handy advanced medical care, and possibly the living environment. Surprisingly many recent articles on the high rise in breast cancer mortality rate showed the impact of family income as more impactful [2].

The 2020 world statistics showed that the middle-income category of developed countries has a very high mortality rate compared to other income groups, and one supportive reason can be the un affordability of expensive diagnostic resources—many Western developed countries raised flags

The associate editor coordinating the review of this manuscript and approving it for publication was Rajeeb Dey.

on the need for early detection screenings for women over 40. As a ground truth to cut the cost and meet the affordability, the countries followed Mammography for regular screenings. An expert radiologist should then analyze the image data for positive or negative confirmation of the cancer [3].

### A. MOTIVATION

The breast X-ray capture is a mammogram, which is analyzed for early tumor detection using various approaches. Unfortunately, the anatomy of the breast is a disappointment that leads to false positive diagnostics. False positive is a case where the breast does not have a cancer tumor, but the diagnostic model classified it as having a tumor [4]. The density of the breast is a vital metrical feature to study because there are many false positive cases with denser and denser breasts. The denseness of the breasts can be due to the radius and size of the fatty tissue. This dense fatty tissue may mislead to tumor tissue, causing a case of false positives. False positives may be over-costing to an economically poor society [5]. Thus, there is a need for an approach to reduce false positives.

### B. PROBLEM DEFINITION

There are cases as well where a mammogram detection approach failed to identify tumors hidden behind the dense tissue. These issues led the radiologist to suggest MRIs and other costly detection approaches for initial screening. The women's financial strength in major developed countries may support the choice of MRI, but there may be more affordable cases for women of economically poor notations. The bottom-line design and proposal for any screening approach should focus on the current financial status of women undergoing the risk [6].

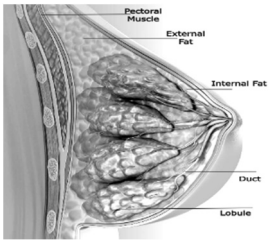


(a)

| Confusion matrix | | Predicted label | |
|---|---|---|---|
| | | 0 | 1 |
| Actual Label | 0 | TN | FP |
| | 1 | FN | TP |

(b)

**FIGURE 1.** (a) Normal breast anatomy (b) false positives.

Supporting the cost-effectiveness of mammograms which can render frequent, low-cost screenings, researchers should aid in reducing the false positive results from mammogram screenings. Recent survey studies from many economically poor notations elicited that most women suffered from false positive test results of the diagnosis approach. A ground truth analysis showed that most false positive cases occurred in women with fatty breasts [7].

### C. NOVELTY OF THE WORK

The proposed article presents a naive, constrained-based algorithm to classify a mammogram image as cancerous, aiming to reduce false positives in Figure 1(b). Most breast mass detection algorithms use Euclidian distance-based measures to diagnose the cancer mass. These distance-based algorithms raised false positives while analyzing the tumor mass overlapped by thick breast fat. Rather than a distance-based, the approach used a distribution-based Bhattacharya's similarity measure to amount these overlapping. The proposed model uses optimal mass transfer theory to study the overlapping distributions by transferring a patch of cancerous mass to a non-cancerous region and vice versa. The Bhattacharya's similarity coefficient calculated for each such mass transfer generated Wasserstein Distribution constraints. A deep learning algorithm is developed (WOMT), which is trained with Wasserstein Distribution constraints to reduce the false positives resulting from fat breasts.

### D. CONTRIBUTIONS

The key aim of this article is to reduce false positives while diagnosing thick breast layers. Outlying the contributions of the proposed approach:

1) An approach of analyzing Bhattacharya's similarity distributions to diagnose the fat overlapping
2) A Deep learning model to reduce the false positives, trained on Wasserstein Distribution constraints.

## II. RELATED WORK

A mammogram image may have unwanted counters and regions, which may not be important for cancer diagnosis. This section presents the related and previous work the literature has shown in addressing the mammogram images, preprocessing the images, and the algorithms used to detect the cancer Tumor [8].

### A. MAMMOGRAM PREPROCESSING

Mammogram researchers have presented several methods for image background removal where excessive, irrelevant image parts are removed from the study [9]. The article used methods like Morphological image transformations, a threshold from Huang's Fuzzy logic, and algorithms like the rolling ball to remove background from the procured images. Background removal approaches like Auto Cropping and Label Omitting were discussed in [10]. A binary opening with a disc-like data structure is used in their approach to remove the background and Labels.

Excluding background using Histogram threshold is discussed in [11], where Gaussian smoothing of the histograms under minimum peaking is applied. The authors also used techniques like Edge detection and active contour growing using the seed point technique for background removal. Their experiments captured more than 40 seed points to generate more accurate images without backgrounds. The background segmentation approach presented by them was 70% accurate.

The breast region without the background is the region of interest with any image processing technique. Automated profiling of the breast for background segmentation is discussed in [12]. The paper discussed approaches like automated region growing and morphological preprocessing to remove digital noises and background. Today's computer-assisted diagnostic systems pre-request many image enhancement techniques for accurate diagnostics. One such in digital mammogram analysis is the breast region segmentation and thorough separation of background. A combined approach of background removal using morphological transformations, histogram threshold, and contour modeling is presented in [13]. Their methodology used local discontinuity of histogram values to determine the final breast boundary.

Women's breasts normally include a thick and intense pectoral muscle, which resembles similar fat tissue. This muscle adversely affects the cancer detection approaches as its gray visualization resembles a cancer tumor. An Automated detection and removal approach of pectoral muscle is presented in [14]. This approach proved accurate in removing the pectoral muscle from the gray mammogram images. Algorithms like hybrid bounding box and region growing were used in [15] to remove the pectoral muscle. The maze segmentation approach used by the authors accurately obtained the best results.

Addressing the need for pectoral muscle removal in any computer-aided detection system, the works in [16] discussed and designed a novel pectoral muscle removal algorithm in digital mammograms. The authors used a combined approach of the Robust Outlying Ratio (ROR) technique with extended NL-Means (ROR-NLM) kind of filters on Discrete Cosine Transform (DCT) for noise and pectoral muscle removal. The approaches were found to be effective in image noise removal.

Breast boundary extraction is the most practiced technique for boundary identification and pectoral muscle removal. A simultaneous method of pectoral muscle removal by identifying the breast boundary is eluded rightly in [17]. A multilevel wavelet decomposition is applied to the images to extract the breast regions perfectly. The generated wavelet coefficients were accurate enough to identify the clear breast border, excluding the pectoral muscle. A robust approach for pectoral muscle segmentation is discussed in [18]. In the work, the authors proposed an approach using contract enhancement of digital images for muscle segmentation. Their experimental results showed 93.4% of segmentation in 295 images.

### B. MASS DETECTION ALGORITHMS

With the advent of computer technology and new AI tools, current research produces many novel methods and algorithms for cancer mass detection. A new image mass classification framework is depicted in [19] using deep learning algorithms. Their results showed a promising future in successfully detecting the cancer mass. Breast density was an important parameter considered by many tumor detection approaches. The seeded region growing algorithm used in [20] showed accurate results of mass detection under various breast densities. A feature-matching algorithm on various breast regions using the Maximally Stable Extremal Regions algorithm is shown in [21]. The algorithm is fully automated without any human assistance. The result analysis of the authors showed that their proposed algorithm has high accuracy when compared to many states of art algorithms.

A computationally efficient and robust algorithm proposed in [22] used a confocal microwave imaging method for cancer mass detection. The results showed by their approach modeled the algorithm's efficiency in detecting even the small and narrow mass regions. The approach discussed in [23] presented a combined CNN feature extraction with extreme learning clustering to detect cancer mass. Their extensive experimentations demonstrated the algorithm's accuracy at about 91.5%. Works presented in [24] used a grasshopper optimization algorithm and optimized feature extraction imbibed in CNN cancer for mass detection. The authors experimentally showed that the proposed algorithm has improved precision and decreased the overall computational cost.

A dual-stage adaptive threshold discussed in [25] proposed an automatic framework for breast cancer detection. The framework used a statistical approach of convolutions for the detection. The neural Net whale optimization algorithm is discussed in [1] to detect breast cancer automatically. The authors showed that their proposed algorithm has the best accuracy compared with various machine learning algorithms.

State-of-the-art literature proposed many machine learning and deep learning algorithms for breast cancer mass detection. The approach discussed in [26] used machine learning algorithms like SVM and Sequential Minimal Optimization (SMO) for breast cancer mass detection. The classifier efficiency is studied by analyzing the true positives and false positives. A hybrid deep learning model is discussed in [27] for breast cancer detection and prediction. The approach took the PCamKaggle dataset and used CNN and GRUs to detect a mass.

## III. THE PROPOSED METHOD

With the immediate need for fast and timely diagnosis of breast cancer, the approach proposed an efficient deep learning Model as the solution to early cancer detection by reducing the false positives of the existing diagnosis algorithms. Mammogram images are breast X-ray images from which early cancer tumors can be diagnosed.

### A. DATA COLLECTION

Kaggle and Digital Mammogram Database, MIAS, are the initial sources of mammogram images. The mammogram images are collected from Git. Four hundred fifty mammo-

gram images, each of 1024 X 1024 size, were part of the proposed analysis.

### B. DATASET PARTITIONING

To support the goal of reducing the false positives, the proposed approach aimed at pulling various constraints by transporting cancer mass patches from image to image. In order to be in line with the various constraints developed, the proposed approach insists on a need for Dataset partitioning into: Cancerous(G1) and Non-Cancerous (G2). The database of images is successfully partitioned into 245 Non-Cancerous and 205 cancerous images. Two hundred forty-five non-cancerous images to 115 non-fatty and 130 fatty images. Two hundred five cancerous images to 105 non-fatty and 100 fatty images, and is presented in Figure 2.

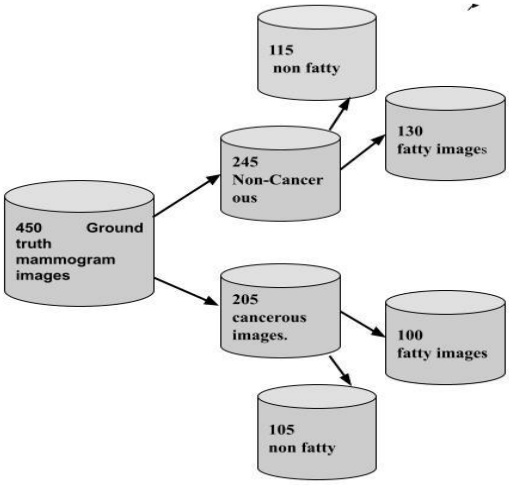


**FIGURE 2.** Data architecture of proposed method.

### C. PROPOSED APPROACH

The proposed approach initially went with preprocessing the images. As a next step, Bhattacharya's distribution is discussed to study and measure the overlapping of various cancerous and non-cancerous mass patches.

#### 1) PRE-PROCESSING

The mammogram images were collected from different repositories, and observed that the images were of different sizes. Removal of the pectoral muscle is the first preprocessing step. After removal, the ratio of the area occupied by the pectoral muscle in the images is different, and an un-fixed position is observed to the left top corner of the gray image. The images are cropped to hold fixed non-pectoral areas, including the breast and mass regions.

We observed that the processed image sizes are inconsistent with unclear regions of breast and mass. So, a need for edge-preserving is identified. The image retargeting approach is followed to achieve image consistency and preserve clear edges. We want to be more informative and fixed to maintain a uniform size of 224 X 224.

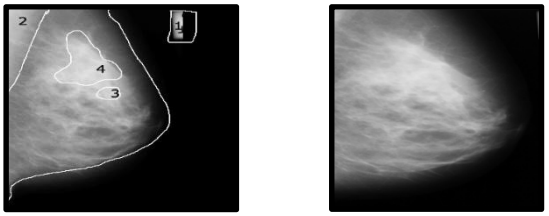


**FIGURE 3.** (a) Image with label-1, pectoral-2, cancer mass-3, breast fat-4 (b) after preprocessing and cropping.

Talking about breast cancer in women, most often, breast cancer originates in milk-producing ducts. The fatty breast ligaments called fatty breast tissues are deceptive to false positive tumor cells. As Figure 3 (a) shows, the cancer mass is most likely to be a fatty mass, which is majorly identified as a false positive. Initial analysis of the image database revealed fatty tissues resemble tumor cells in gray images. As seen in Figure 1 breast anatomy, the internal fat is where the duct cell falls. This internal fat is more closely resembled tumor mass. Unless assisted with an accurate diagnostic approach, it still results in false positives, thus a great need for careful and better image preprocessing and diagnostic methodology.

The literature showed many image patch transportation techniques to disseminate the fat mass regions with the tumor mass regions, where a patch matching is analyzed and observed. Most existing image patch matching methods used Euclidean-based mass patch delineation for easy diagnostic assistance. This approach uses a template T of tumor mass, which can be 8 X 8 or more in size, where this template is flipped on the cancerous image I, left to right or top to bottom, and calculates the similarity between T and the breast mass regions. The high similarities are categorized as suspected cancer mass. Results of many works showed even these patch flip methods with high similarities, which were diagnosed as positive initially, went negative after a trail of the same runs. Here the observed images were found to be fattier. The similarity measure used for patch matching is the Euclidean distance D(i,j) given in Equation.

$$D(i,j) = \sum_{m=1}^{M} \sum_{n=1}^{N} [P(m,n) - T(m,n)]^2 \quad (1)$$

Here D(i,j) is the corresponding Euclidean distance between the template T and image patch P for i=1 to M and j=1 to N. For templates of size 7 X 7, m and n are the width and height which are respectively 7. P(m,n) and T (m,n) are the image pixel values of the patch and template respectively. Figure 4 shows two image patches at two regions, P1=R1 and P2=R2 measuring similarity by flip using template T, with tumor mass.

The Euclidean distance metric failed in cases where the tumor mass is bonded and overlapped with the fatty mass of the breast. Those seeded patches are misclassified as tumor masses or breast fats. The image shown in Figure 4 is a ground truth image where cancer mass is diagnosed at two regions, R1 and R2. A sample template patch T is obtained from a

ground truth image having tumor mass. The region R1 with tumor mass patch P1, this patch P1 found to be having high similarity with the tumor mass, template T, when measured using Euclidean distance.

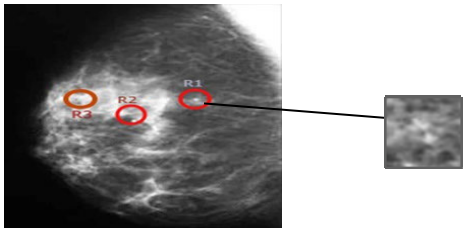


**FIGURE 4.** Ground truth image with R1: tumor mass patch, R2: tumor mass overlapped by fatty breast, R3: fatty mass alone.

However, the same similarity metric failed when the patch at region R2 was compared with Template T, where the measure resulted in less similarity. Because of region R2 though it has tumor mass, this mass is encompassed and overlapped by thick breast fat, and thus Euclidean distance failed to capture the similarity. Here the patch is identified non -cancerous. Region R3 is not with any tumor mass, and the Euclidean distance approach identified the similarity as almost equal because R3 has a fattier overlapped region and, thus, a case of false positive. A countermeasure is to analyze the distributions of the image patches and find how much the overlapping is to apply a better patch transportation theory.

### 2) BHATTACHARYA'S DISTRIBUTION: MEASURING OVERLAPPING

As a case of concern is to reduce false positives resulting from heavy, fatty breasts, we want to measure the kind of overlapping of breast patches P with tumor mass template T.

Analyzing the false positive rate by Euclidean distance, the approach used similarity by Bhattacharya's distance metric to analyze the distribution similarity of two or more mass patches. Bhattacharya's distance is used to measure the amount of overlap between tumor mass and breast fat. For any two tumor mass patches P1, and P2 on a domain of pixels X, the Bhattacharya's similarity is given by,

$$BD(P1, P2) = -ln(BC(P1, P2)) \tag{2}$$

where BC(P1, P2) is the Bhattacharya's co-efficient given by

$$BC(P1, P2) = \int_X \sqrt{P1(x), P2\,(x)}dx \tag{3}$$

With $0 \leq$ BC $\leq 1$, the Bhattacharyya coefficient BC. (P1,P2) quantifies the overlapping of two random statistical sample Patches P1, and P2. When BC=0, the patches are completely dissimilar, BC=1, the patches are completely similar.

Running hypothesis testing on the distributions showed that when the Bhattacharyya Coefficient between two distributions is $< 0.05$, the distributions are significantly different. When this coefficient is $>0.95$, both distributions are significantly similar. Values between these two thresholds show the probability of overlap between the distributions. With the application of Bhattacharya's similarity metric over collected patches and ground truth templates. Let P={P1, P2, P3,...}; T={T1, T2, T3,...} be the patches corresponding to breast fat regions and Tumor templates. We collected these patches from various fat regions of the breast, both from cancerous and non-cancerous images.

A novel data structure is built to hold these patches and ground truth templates, called the Patch stack as shown in Figure 5. Finding the Bhattacharya's coefficient for BC(P,T) measures the overlap of the breast fat regions and Tumor.

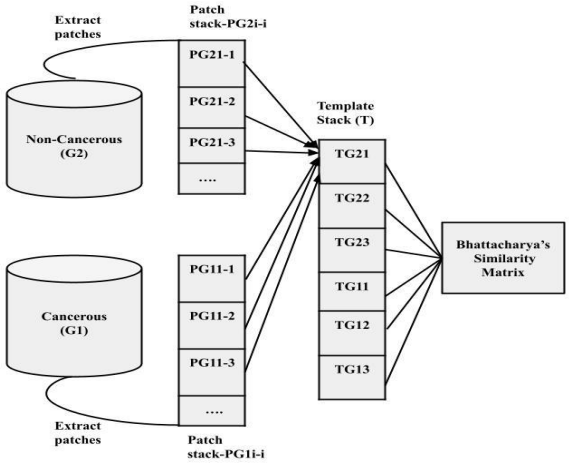


**FIGURE 5.** Data structure- multi Patch stack for finding bhattacharya's similarity.

This multi-patch stacking data structure is used to stack templates of various breast tumor mass regions, to be compared with the various breast patches. Out of many collected patch samples and templates, here we present an analysis of six sample template patches from original ground truth cancerous and non-cancerous images with the support of computer-aided diagnosis (CAD). This is shown in Table 1. Table 2 shows the description of the templates.

**TABLE 1.** Ground truth sample patch templates.

| Template Id | TG21 | TG22 | TG23 | TG11 | TG12 | TG13 |
|---|---|---|---|---|---|---|
| Sample ground truth Image (224X224) | 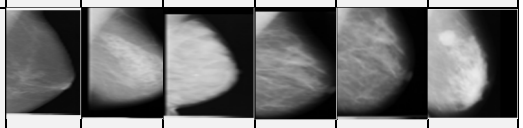 | | | | | |
| Patch template (T) (8X8) |  | | | | | |

From the 245 Non-Cancerous (G2) and 205 Cancerous (G1) images, we collected nearly 784 patches each of size $8 \times 8$ pixels from each image. For each image, we stacked all the 784 patches and captured the similarity value with the patches in the Template stack as described in Tables 1 and 2.

The Bhattacharya's similarity matrix is constructed and A sample of the values is shown in table 3 and respective tables below show overlapping collected on one Image from Non-Cancerous and one image from cancerous Databases. Among the 784 patches of one Image, we randomly analyzed an array of continuous patches to study the overlapping of T and P using Bhattacharya's co-efficient as included below

**TABLE 2.** Descriptions of table 1 templates.

| Template Type | Template Id | Region |
|---|---|---|
| Non-Cancerous (G2) | TG21 | Normal breast region, no fat, no tumor mass |
| | TG22 | Normal breast region with, moderate fat, no tumor mass |
| | TG23 | Normal breast region with heavy fat, no tumor mass |
| Cancerous(G1) | TG11 | Normal breast region, no fat, with tumor mass |
| | TG12 | Normal breast region with, moderate fat, with tumor mass |
| | TG13 | Normal breast region with heavy fat, tumor mass |

The nomenclature followed here is, BC (TG2-i, PG21-i) (Bhattacharya's co efficient giving the overlapping of T and P), G2-1(Image 1 from Non-cancerous database), G1-1 (Image 1 from Cancerous Database), TG2i (Non-cancerous mass Template), TG1i (Cancerous mass Template), PG2i-j (array of j patches from non-cancerous Image i), PG1i-j (array of j patches from cancerous Image i).

**TABLE 3.** Bhattacharya's co efficient BC (TG2-i, PG21-j)-no fat.

| Bhattacharya's co efficient BC(TG2-i, PG21-j)-No Fat | | | | | | | |
|---|---|---|---|---|---|---|---|
| T/Non Cancerous Patches (G2-1) | PG21-64 | PG21-65 | PG21-66 | PG21-67 | PG21-68 | PG21-69 | PG21-70 |
| TG2-1 | 0.95 | 0.81 | 0.87 | 0.84 | 0.91 | 0.96 | 0.86 |
| TG2-2 | 0.41 | 0.48 | 0.45 | 0.51 | 0.53 | 0.42 | 0.61 |
| TG2-3 | 0.40 | 0.39 | 0.32 | 0.48 | 0.50 | 0.43 | 0.36 |
| TG1-1 | 0.21 | 0.26 | 0.22 | 0.24 | 0.23 | 0.19 | 0.32 |
| TG1-2 | 0.32 | 0.31 | 0.39 | 0.30 | 0.29 | 0.32 | 0.28 |
| TG1-3 | 0.20 | 0.25 | 0.22 | 0.25 | 0.23 | 0.20 | 0.42 |

The distribution overlapping is completely dependent on the precision of Bhattacharyya Coefficient. The precision of the Bhattacharyya Coefficient is directly proportional to the array of number of continuous pixels (n X n). If the array size is too high, the overlap will be underestimated. So the proposed approach uses an array of 7-10 sizes each with a patch (P) of $8 \times 8$ pixels. Displayed are the results on an array of 7 sizes.

Table 3 shows Bhattacharya's co-efficient BC for Non-Cancerous patches (PG21-j) and six ground truth template patches (TG2i). TG2-1 is a patch showing a normal breast region, no fat, and no tumor mass. We showed a sample of array patches of size 7, from 64-70. The Bhattacharya's co-efficient BC of TG2-1 with these seven patches is found to be very high. Showing the template patch, TG2-1 is almost overlapping and similar to an array of patches. Also, TG1-1 has less similarity though being non-fatty, with cancerous mass. These are the two cases in the experimental setup.

**TABLE 4.** Bhattacharya's co efficient BC(TG2-i, PG22-j)-moderate fat.

| Bhattacharya's co efficient BC(TG2-i, PG22-j)-Moderate Fat | | | | | | | |
|---|---|---|---|---|---|---|---|
| T/Non Cancerous Patches (G2-1) | PG22-218 | PG22-219 | PG22-220 | PG22-221 | PG22-222 | PG22-223 | PG22-224 |
| TG2-1 | 0.15 | 0.21 | 0.18 | 0.24 | 0.31 | 0.26 | 0.16 |
| TG2-2 | 0.86 | 0.82 | 0.90 | 0.88 | 0.69 | 0.81 | 0.80 |
| TG2-3 | 0.79 | 0.75 | 0.81 | 0.82 | 0.78 | 0.67 | 0.63 |
| TG1-1 | 0.20 | 0.32 | 0.28 | 0.34 | 0.29 | 0.28 | 0.31 |
| TG1-2 | 0.30 | 0.31 | 0.32 | 0.31 | 0.39 | 0.32 | 0.38 |
| TG1-3 | 0.22 | 0.27 | 0.32 | 0.45 | 0.13 | 0.20 | 0.46 |

**TABLE 5.** Bhattacharya's co efficient BC(TG2-i, PG23-j)- heavy fat.

| Bhattacharya's co efficient BC(TG2-i, PG23-j)- Heavy Fat | | | | | | | |
|---|---|---|---|---|---|---|---|
| T/Non Cancerous Patches (G2-1) | PG23-316 | PG23-317 | PG23-318 | PG23-319 | PG23-320 | PG23-321 | PG23-322 |
| TG2-1 | 0.15 | 0.21 | 0.18 | 0.24 | 0.31 | 0.26 | 0.16 |
| TG2-2 | 0.56 | 0.72 | 0.78 | 0.78 | 0.69 | 0.81 | 0.80 |
| TG2-3 | 0.89 | 0.74 | 0.86 | 0.82 | 0.78 | 0.97 | 0.93 |
| TG1-1 | 0.20 | 0.32 | 0.28 | 0.34 | 0.29 | 0.28 | 0.31 |
| TG1-2 | 0.30 | 0.31 | 0.32 | 0.31 | 0.39 | 0.32 | 0.38 |
| TG1-3 | 0.22 | 0.27 | 0.32 | 0.45 | 0.13 | 0.20 | 0.46 |

**TABLE 6.** Bhattacharya's co efficient BC(TG2-i, PG11-j) - no fat.

| Bhattacharya's co efficient BC(TG2-i, PG11-j) - No Fat | | | | | | | |
|---|---|---|---|---|---|---|---|
| T/Cancerous Patches (G11) | PG11-78 | PG11-79 | 9PG11-80 | PG11-81 | PG11-82 | PG11-83 | PG11-84 |
| TG2-1 | 0.15 | 0.21 | 0.18 | 0.24 | 0.31 | 0.26 | 0.16 |
| TG2-2 | 0.16 | 0.12 | 0.28 | 0.28 | 0.19 | 0.28 | 0.30 |
| TG2-3 | 0.30 | 0.25 | 0.21 | 0.32 | 0.31 | 0.29 | 0.33 |
| TG1-1 | 0.95 | 0.81 | 0.87 | 0.84 | 0.91 | 0.96 | 0.86 |
| TG1-2 | 0.30 | 0.31 | 0.32 | 0.31 | 0.39 | 0.32 | 0.38 |
| TG1-3 | 0.22 | 0.27 | 0.32 | 0.45 | 0.13 | 0.20 | 0.46 |

From the tables, it is observed that the tables above TG2-1 with patches of Moderate fat and heavy fat, non-cancerous,

**TABLE 7.** Bhattacharya's co efficient BC(TG2-i, PG12-j) - moderate fat.

| Bhattacharya's co efficient BC(TG2-i, PG12-j) - Moderate Fat | | | | | | | |
|---|---|---|---|---|---|---|---|
| T/Cancerous Patches (G1-1) | PG12 - 441 | PG12 -442 | PG12 -443 | PG12 -444 | PG12 -445 | PG12 -446 | PG12 -447 |
| TG2-1 | 0.15 | 0.21 | 0.18 | 0.24 | 0.31 | 0.26 | 0.16 |
| TG2-2 | 0.36 | 0.32 | 0.20 | 0.28 | 0.29 | 0.31 | 0.30 |
| TG2-3 | 0.69 | 0.65 | 0.51 | 0.52 | 0.58 | 0.57 | 0.43 |
| TG1-1 | 0.20 | 0.32 | 0.28 | 0.34 | 0.29 | 0.28 | 0.31 |
| TG1-2 | 0.88 | 0.85 | 0.91 | 0.89 | 0.79 | 0.87 | 0.85 |
| TG1-3 | 0.21 | 0.25 | 0.29 | 0.42 | 0.19 | 0.27 | 0.15 |

**TABLE 8.** Bhattacharya's co efficient BC(TG2-i, PG13-j)- heavy fat.

| Bhattacharya's co efficient BC(TG2-i, PG13-j)- Heavy Fat | | | | | | | |
|---|---|---|---|---|---|---|---|
| T/Cancerous Patches (G11) | PG13 - 477 | PG13 -478 | PG13 -479 | PG13 -480 | PG13 -481 | PG13 -482 | PG13 -483 |
| TG2-1 | 0.15 | 0.21 | 0.18 | 0.24 | 0.31 | 0.26 | 0.16 |
| TG2-2 | 0.56 | 0.72 | 0.78 | 0.78 | 0.69 | 0.81 | 0.80 |
| TG2-3 | 0.90 | 0.95 | 0.81 | 0.82 | 0.88 | 0.87 | 0.93 |
| TG1-1 | 0.20 | 0.32 | 0.28 | 0.34 | 0.29 | 0.28 | 0.31 |
| TG1-2 | 0.30 | 0.31 | 0.32 | 0.31 | 0.39 | 0.32 | 0.38 |
| TG1-3 | 0.89 | 0.75 | 0.87 | 0.82 | 0.78 | 0.97 | 0.93 |

have less value of Bhattacharya's coefficient. Concaving the image is non-cancerous. The experimental calculations for Bhattacharya's coefficient and the values obtained on various patches and defined templates made us run a hypothesis testing on two observed values, 0.85 and 0.5, with 90% probability covered. These test case results provided us a thorough, fair configuration of patch mass constraints as given below:

For the case of No fat and Moderate fat, non-cancerous:

$$Avg(BC(TG2-i, PG21-j)) > 0.85, \tag{4}$$

$$Avg(BC(TG2-i, PG21-j)) < 0.5; for i = 1, 2, 3 \text{ and } j \times \text{in array of size } 7 \tag{5}$$

For the case of No fat and Moderate fat, cancerous:

$$Avg(BC(TG1-i, PG11-j)) < 0.5; \tag{6}$$

$$Avg(BC(TG1-i, PG11-j)) > 0.85, for\ i = 1, 2, 3 \text{ and } j \times \text{in array of size } 7 \tag{7}$$

For the case of Heavy fat, cancerous:

$$Avg(BC(TG1-i, PG11-j)) > 0.85; \tag{8}$$

$$Avg(BC(TG1-i, PG11-j)) > 0.85, for i = 1, 2, 3 \text{ and } j \times \text{in array of size } 7 \tag{9}$$

The concerning fact here is that in the case of heavy fat, the Bhattacharya's co-efficient resulted in high similarity showing the heavy overlapping of the cancer mass with the heavy fat mass. When we observed the image database derived from these templates, we found these are from false positives.

### 3) PROPOSED APPROACH

The case of maximal overlapping of the tumor mass with fatty patch: Wasserstein's Optimal mass transfer theory (WOMT)From the analytical runs on various images for Bhattacharya's coefficient, we obtained nearly similar and approximately equal coefficients for the case of Heavy fat in both non-cancerous and cancerous analytical results. The thick breast fat tissue is affecting diagnostics. As we do not know how the tumor mass overlaps with the thick fat tissue and vice versa, the proposed approach used Wasserstein's transport theory to diagnose the tumor. Once overlapping is measured using Bhattacharya's coefficient, the proposed method uses Wasserstein's Optimal mass transfer theory [7] (WOMT), where the transfer of patch mass of tumor is analyzed to arrive at proposed WOMT constraints for tumor classification.

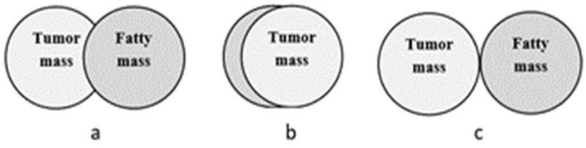


**FIGURE 6.** (a) ROI1 (b) ROI2 (c) ROI3.

The observations included transferring a patch template of various cancer masses to various non-cancerous and cancerous fatty images and simulating Wasserstein's distributions. We took patches of various sizes and a stack of 7 to 10 templates to address optimal mass transfer.

Wasserstein's Optimal mass transfer theory (WOMT), the proposed approach, used Wasserstein's distributions on top of optimal mass transfer to arrive at WOMT constraints. In contrast, the approach used the Optimal mass transport (OMT) theory. Recently OMT had a practical impact on analyzing medical images.

Once the overlapping of the fatty tumor and the fatty patch is measured, the proposed approach takes advantage of measuring this shift of overlapped cancer mass about regions of interest (ROI):

1) ROI1: Partial overlap of cancer mass patch with fatty breast patch.
2) ROI2: Full overlap of cancer mass patch with fatty breast patch.
3) ROI3: No overlap of cancer mass patch with fatty breast patch.

Mass shift need not be studied at the full overlap. We want to study the mass shift only for ROI1 and ROI3. The proposed constraints are derived by analyzing the probability distributions of all the mass shifts among these ROIs. These constraints then go out to classify medical images as cancerous and non-cancerous.

From point masses to Wasserstein cumulative distributions

**$L^r$- Wasserstein distance**:

Let S1 and S2 denote two probability spaces with measures $\mu 1$ and $\mu 2$, respectively, and let C(s1, s2) denote the transportation cost for moving one unit of mass from

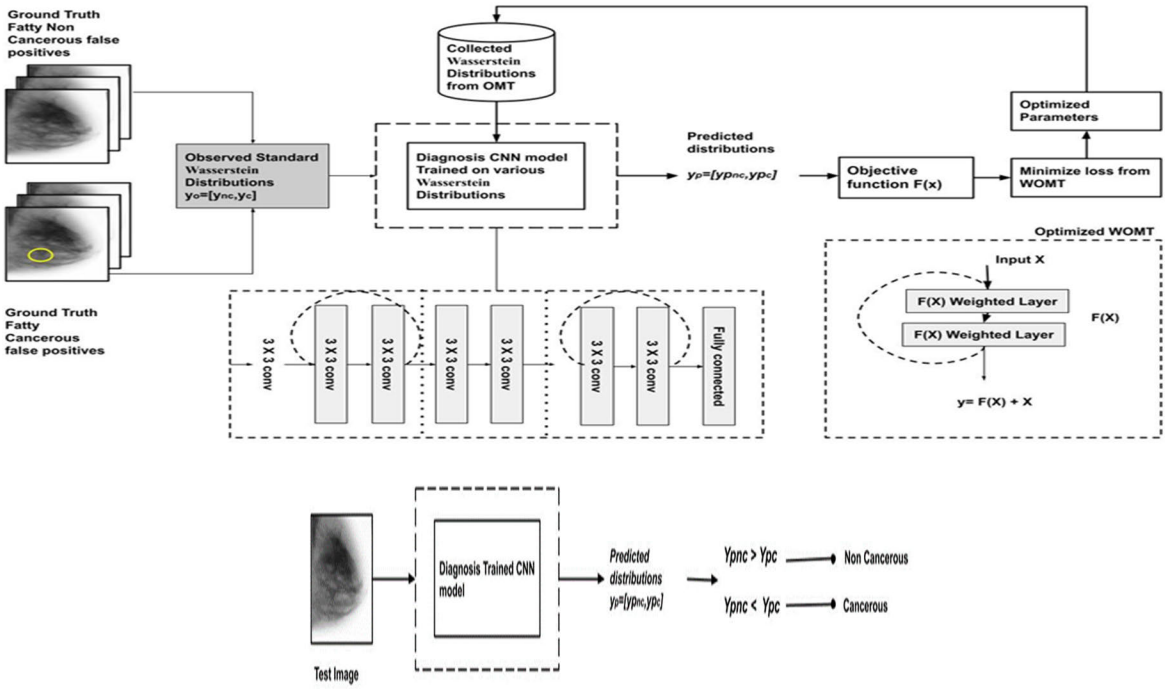


**FIGURE 7.** WOMT architecture.

s1 ∈ S1 to s2 ∈ S2. The objective of OMT is to minimize the total mass shifting cost of the functional map F: S1 → S2, and is given by total shifting cost:

$$Totalshiftcost = \int SC(S, F(s))\mu(ds) \tag{10}$$

As a metric to measure the mass shift, the approach took advantage of the Lr- Wasserstein distance between $\mu 1$ and $\mu 2$ on an image space $\mathbb{R}$d. This section includes how Wasserstein cumulative distributions are arrived upon from point masses.

Point masses (degenerate distributions):

For the image data, with a defined pixel space, which can be here taken as a patch (p), a degenerate distribution is probability distribution only at a single pixel.

Let $\mu 1 = \omega p1$, $\mu 2 = \omega p2$ located at two image pixels p1,p2 in $\mathbb{R}$ defined, so we can find the point mass at p1, p2 as $\omega$(p1,p2) which is located at (p1,p2) ∈ $\mathbb{R}$2.

For any r ≥ 1

Lr- Wasserstein distance between $\mu 1$ and $\mu 2$ is:

$$Wr(\mu 1, \mu 2) = |p1 - p2| \tag{11}$$

Using the normed Euclidean as distance metric, then

$$Wr(\mu 1, \mu 2) = ||p1 - p2||^2 \tag{12}$$

**$L^2$Wasserstein distance**:

In the proposed work, we are taking advantage of Lr Wasserstein distance for r=2. The defined distance metric is intended to evaluate the probability distribution of the patch data P1 with a total mass of m1. The approach included finding patch-based Gaussian measures km1 and km2 ∈ $\mathbb{R}$l, mean and Covariance matrix MCov(i) for i = 1,2, which are needed for the distributions from various ROI shifts.

Let sample data in the native spaces of template T, and fatty area F be X = [x1,x2, ⋯, xm] and Y = [y1, y2, ⋯, ym] ∈ $\mathbb{R}^d$ where m=1,2,3,4…m are respective patch sizes corresponding to various masses.

The $L^2$-Wasserstein distance between the two distributions is given by

$$W_2(km_1, km_2)^2 = ||\mu 1 - \mu 2||^2 + T_{\text{race}}(Cov_1 + Cov_2 - 2(Cov_2 Cov1)^{1/2} \tag{13}$$

where $T_{race}$ is the trace, which is here the sum of the diagonal elements of the covariance matrices.

The mean $\mu$ of the pixel masses of the feature space is given by:

$$\mu = \frac{1}{m}\sum_1^m t\,(xi) = tX \tag{14}$$

The covariance matrix of the pixel masses of the feature space is given by:

$$M_{\text{Cov(i)}} = \frac{1}{m}\sum_{i=1}^m (t\,(xi) - \mu)\,(t\,(xi) - \mu) \tag{15}$$

Wasserstein cumulative distributions constraints:

For the mean masses $\mu 1$, $\mu 2$ ∈Pr($\mathbb{R}$) with probability measure P on $\mathbb{R}$, denote the cumulative distributions on the pixel sample spaces X,Y as F(X), F(Y). We now define the transport problem on the pixels probability mass as: for a patch amount p1 of mass $\mu$(x) distributed on pixel space

X, if transported to a distribution on pixel space Y, then the Lr- Wasserstein distance between $\mu 1$ and $\mu 2 \in \Pr(\mathbb{R})$ is:

$$Wr(\mu 1, \mu 2) = (\int_0^1 |F - 1X(p1) - F - 1Y(p1)|rdp1)1/r \tag{16}$$

From equation 11, The Wasserstein constraints are the bounded Wasserstein distributions giving the difference between the mean overlapping. The derived Wasserstein constraints

Partial overlap of malignant cancer mass patch with fatty breast patch:

$$W_{p1}(\mu 1, \mu 2) \leq W_{p2}(\mu 1, \mu 2) \tag{17}$$

Full overlap of malignant cancer mass patch with fatty breast patch:

$$W_{p1}(\mu 1, \mu 2) > W_{p2}(\mu 1, \mu 2) \tag{18}$$

The proposed objective function from WOST is to Minimize F(X), by applying various transportations of cancerous mass to non-cancerous masses. F(X) is given by

$$F(X) = |W_{p1}(\mu 1, \mu 2) - W_{p2}(\mu 1, \mu 2)| \tag{19}$$

#### 4) ARCHITECTURE OF PROPOSED WOMT

Initial CNN [28] was modeled on the ground truth images to collect the false positives from cancerous and non-cancerous Databases. Then these false positive images are subjected to collect the observed Wasserstein cumulative distributions. A retraining phase on CNN is again initiated, where the model is trained with the OMT Wasserstein cumulative distribution constraints as given in equation 19.

The predicted distributions are compared with observed standard distributions. The model test loss is evaluated. This loss is minimized by patch-based OMT, and optimized Wasserstein cumulative distribution constraints are obtained. The WOMT architecture shown in Figure 8 shows how the fatty images are classified as cancerous and non-cancerous. The proposed method steps are as in algorithm 1.

**Algorithm 1** WOMT

1. Collect patches and templates P={P1,P2,P3,…};
   T={T1,T2,T3,…}
2. Generate Bhattacharya's co efficient BC(TG2-i, PG21-i)
3. If Avg(BC(TG1-i,PG11-j)) > 0.85;
   Avg(BC(TG1-i,PG11-j)) > 0.85
   Then identified maximal overlapping, apply WOST
4. Run CNN to collect FPs
5. Observed Standard Wasserstein Distributions
   yo=[ync,yc]
6. Apply Trained CNN with WOMT constraints
7. If Ypnc>Ypc then Non Cancerous
   If Ypnc< Ypc then cancerous

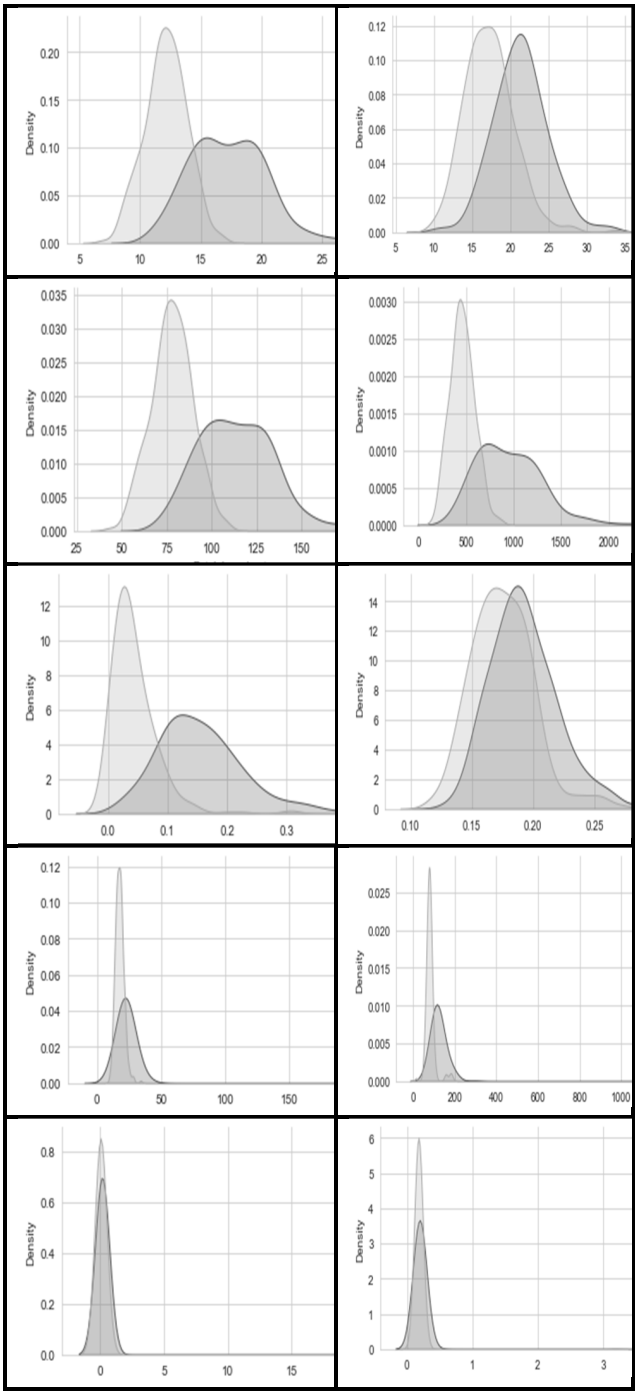


**FIGURE 8.** Sample predicted distributions from WOMT.

## IV. EXPERIMENTAL RESULTS

We conducted experiments using CNN modeled by python codes and Wasserstein cumulative distribution constraints modeled by R codes. The first step insisted on collecting the false positives from a classifier CNN. Preprocessed the images. We input the preprocessed images to a trained CNN model for classification. The training data image information while using CNN is displayed in Table 9.

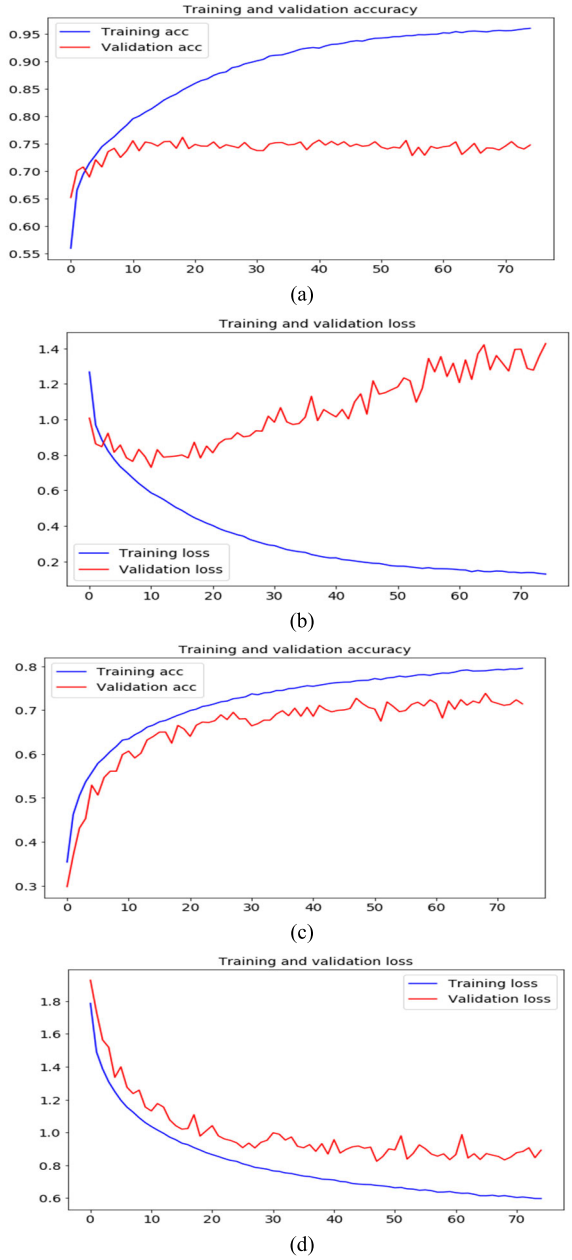


**FIGURE 9.** (a) (b) Train and test loss from CNN, (c) (d) train and test loss from WOMT trained CNN.

**TABLE 9.** CNN training phase parameters.

| | |
|---|---|
| Initial image size | 1024 X 1024 |
| Resized image | 224 X 224 |
| Kernel size | 3 X 3 |
| Convolutional | 32 |
| Learning rate (l) | 0.01 |

We observed that the fatty images resulted in more of false positives. The false positives obtained in either case are shown in the confusion matrices of Table 10.

We found a good lot of false positives from the fatty images. We collected the false positive images to database

**TABLE 10.** CNN confusion matrix – false positives.

| Confusion matrix non-cancerous fatty | | Predicted label | |
|---|---|---|---|
| | | 0 | 1 |
| Actual Label | 0 | 37 | 56 |
| | 1 | 4 | 33 |

| Confusion matrix cancerous fatty | | Predicted label | |
|---|---|---|---|
| | | 0 | 1 |
| Actual Label | 0 | 28 | 41 |
| | 1 | 1 | 30 |

FP. The train loss and accuracy of initial CNN run is shown in Figure 9.

In the next phase we applied the proposed approach on FP database. We collected fatty patches Pi of varied masses from false positives of cancerous applied OMT on to non-cancerous fatty images. The WOMT constraints were captured by minimizing the F(X). Sequentially the CNN was trained to reduce the test loss with optimal WOMT constraints. The final trained CNN is used for test image classification. We observed that the WOMT trained CNN reduced false positives. The train loss and accuracy of WOMT trained CNN is shown in Figure 9. Sample predicted distributions from WOMT are shown in Figure 9. The loss and accuracy shown in figure 9, shows the proposed approach successfully reduced false positives and resulted in reducing the test loss.

## V. CONCLUSION AND FUTURE SCOPE

Women life suffered from deadly breast cancer is the main focus. The cause reasons can be many among the living habits to diversified ecological affects. Invasive tumors spread from tissue to tissue, with high chances of causing new tumors. Medical diagnosis approach like CT scan has paved for early and successful detection of the cancerous tumors. But there were cases where even diagnosis with CT scan images failed and resulted in many false positives. In economically backward countries these false positives are nightmare of women's concern and bloated the affordability. Due to change in biological metabolism the growth of the breast fat in women to considerably abnormal size is the main cause for false positives. In many of the images under study, this huge thick breast fat layer led to the raise of misclassification rate. Rendering a societal help is a need for accurate mechanism that can reduce the false positives at an initial diagnosis itself. The proposed method introduces a novel Wasserstein Distribution constraint that are obtained from mass transfer of cancerous patches to non-cancerous patches. The experimental simulations with deep learning model trained with these constraints resulted in reduced false positives.

The proposed article presents a naive constrained based algorithm to classify a mammogram image as cancerous, aiming reduced false positives. Initial Euclidian distance-based measures to diagnosis the cancer mass raised false

positives while analyzing the tumor mass overlapped by thick breast fat.

The proposed approach used Bhattacharya's similarity measure to amount these overlapping. We developed deep learning algorithm (WOMT) which is trained with Wasserstein Distribution constraints to reduce the false positives resulted from fat breasts.

The proposed work explained the methodology on different regions $ROI_1$ and $ROI_2$. However, this work didn't include analysis on region of full overlap the $ROI_3$, which we want to present as a future work.

## REFERENCES


[1] L. Shen, L. R. Margolies, J. H. Rothstein, E. Fluder, R. McBride, and W. Sieh, "Deep learning to improve breast cancer detection on screening mammography," *Sci. Rep.*, vol. 9, no. 1, p. 12495, Aug. 2019, doi: 10.1038/s41598-019-48995-4.

[2] N. M. U. Din, R. A. Dar, M. Rasool, and A. Assad, "Breast cancer detection using deep learning: Datasets, methods, and challenges ahead," *Comput. Biol. Med.*, vol. 149, Oct. 2022, Art. no. 106073, doi: 10.1016/j.compbiomed.2022.106073.

[3] E. A. Mohamed, E. A. Rashed, T. Gaber, and O. Karam, "Deep learning model for fully automated breast cancer detection system from thermograms," *PLoS ONE*, vol. 17, no. 1, Jan. 2022, Art. no. e0262349, doi: 10.1371/journal.pone.0262349.

[4] M. F. Mridha, M. A. Hamid, M. M. Monowar, A. J. Keya, A. Q. Ohi, M. R. Islam, and J.-M. Kim, "A comprehensive survey on deep-learning-based breast cancer diagnosis," *Cancers*, vol. 13, no. 23, p. 6116, Dec. 2021, doi: 10.3390/cancers13236116.

[5] K. S. Priyanka, "A review paper on breast cancer detection using deep learning," *IOP Conf. Ser., Mater. Sci. Eng.*, vol. 1022, no. 1, Jan. 2021, Art. no. 012071, doi: 10.1088/1757-899X/1022/1/012071.

[6] N. Khuriwal and N. Mishra, "Breast cancer diagnosis using deep learning algorithm," in *Proc. Int. Conf. Adv. Comput., Commun. Control Netw. (ICACCCN)*, Oct. 2018, pp. 98–103, doi: 10.1109/ICACCCN.2018.8748777.

[7] Z. Su, Y. Wang, R. Shi, W. Zeng, J. Sun, F. Luo, and X. Gu, "Optimal mass transport for shape matching and comparison," *IEEE Trans. Pattern Anal. Mach. Intell.*, vol. 37, no. 11, pp. 2246–2259, Nov. 2015, doi: 10.1109/TPAMI.2015.2408346.

[8] S. Sreedevi and E. Sherly, "A novel approach for removal of pectoral muscles in digital mammogram," *Proc. Comput. Sci.*, vol. 46, pp. 1724–1731, Jan. 2015, doi: 10.1016/j.procs.2015.02.117.

[9] *Preprocessing of Breast Cancer Images to Create Datasets for Deep-CNN | IEEE Journals & Magazine | IEEE Xplore*. Accessed: Jan. 18, 2023. [Online]. Available: https://ieeexplore.ieee.org/document/9352727

[10] *Preprocessing of Digital Mammogram Image Based on Otsu's Threshold | American Academic Scientific Research Journal for Engineering, Technology, and Sciences*. Accessed: Jan. 18, 2023. [Online]. Available: https://asrjetsjournal.org/index.php/American_Scientific_Journal/article/view/3476

[11] Z. Chen, "Segmentation of the breast region with pectoral muscle removal in mammograms," Dept. Comput. Sci., Aberystwyth Univ., U.K., Tech. Rep.

[12] J. Nagi, S. A. Kareem, F. Nagi, and S. K. Ahmed, "Automated breast profile segmentation for ROI detection using digital mammograms," in *Proc. IEEE EMBS Conf. Biomed. Eng. Sci. (IECBES)*, Nov. 2010, pp. 87–92, doi: 10.1109/IECBES.2010.5742205.

[13] T. Ojala, J. Nöppi, and O. Nevalainen, "Accurate segmentation of the breast region from digitized mammograms," *Comput. Med. Imag. Graph.*, vol. 25, no. 1, pp. 47–59, Jan. 2001, doi: 10.1016/S0895-6111(00)00036-7.

[14] *Automatic Pectoral Muscle Removal in Mammograms*. Accessed: Jan. 18, 2023. [Online]. Available: https://link.springer.com/article/10.1007/s12530-019-09310-8

[15] E. M. H. Saeed and H. A. Saleh, "Pectoral muscles removal in mammogram image by hybrid bounding box and region growing algorithm," in *Proc. Int. Conf. Comput. Sci. Softw. Eng. (CSASE)*, Apr. 2020, pp. 146–151, doi: 10.1109/CSASE48920.2020.9142055.

[16] B. Mughal, N. Muhammad, M. Sharif, T. Saba, and A. Rehman, "Extraction of breast border and removal of pectoral muscle in wavelet domain," *Biomed. Res.*, vol. 28, no. 11, pp. 5041–5043, Jun. 2017, Accessed: Jan. 18, 2023. [Online]. Available: https://www.alliedacademies.org/abstract/extraction-of-breast-border-and-removal-of-pectoral-muscle-in-wavelet-domain-7608.html

[17] M. Mustra and M. Grgic, "Robust automatic breast and pectoral muscle segmentation from scanned mammograms," *Signal Process.*, vol. 93, no. 10, pp. 2817–2827, Oct. 2013, doi: 10.1016/j.sigpro.2012.07.026.

[18] S. J. Mambou, P. Maresova, O. Krejcar, A. Selamat, and K. Kuca, "Breast cancer detection using infrared thermal imaging and a deep learning model," *Sensors*, vol. 18, no. 9, p. 2799, Aug. 2018, doi: 10.3390/s18092799.

[19] N. Shrivastava and J. Bharti, "Breast tumor detection and classification based on density," *Multimedia Tools Appl.*, vol. 79, nos. 35–36, pp. 26467–26487, Sep. 2020, doi: 10.1007/s11042-020-09220-x.

[20] S. A. Hassan, M. S. Sayed, M. I. Abdalla, and M. A. Rashwan, "Detection of breast cancer mass using MSER detector and features matching," *Multimedia Tools Appl.*, vol. 78, no. 14, pp. 20239–20262, Jul. 2019, doi: 10.1007/s11042-019-7358-1.

[21] X. Li and S. C. Hagness, "A confocal microwave imaging algorithm for breast cancer detection," *IEEE Microw. Wireless Compon. Lett.*, vol. 11, no. 3, pp. 130–132, Mar. 2001, doi: 10.1109/7260.915627.

[22] *Breast Cancer Detection Using Extreme Learning Machine Based on Feature Fusion With CNN Deep Features | IEEE Journals & Magazine | IEEE Xplore*. Accessed: Jan. 18, 2023. [Online]. Available: https://ieeexplore.ieee.org/document/8613773

[23] Z. Sha, L. Hu, and B. D. Rouyendegh, "Deep learning and optimization algorithms for automatic breast cancer detection," *Int. J. Imag. Syst. Technol.*, vol. 30, no. 2, pp. 495–506, Jun. 2020, doi: 10.1002/ima.22400.

[24] J. Anitha, J. D. Peter, and S. I. A. Pandian, "A dual stage adaptive thresholding (DuSAT) for automatic mass detection in mammograms," *Comput. Methods Programs Biomed.*, vol. 138, pp. 93–104, Jan. 2017, doi: 10.1016/j.cmpb.2016.10.026.

[25] H. Fang, H. Fan, S. Lin, Z. Qing, and F. R. Sheykhahmad, "Automatic breast cancer detection based on optimized neural network using whale optimization algorithm," *Int. J. Imag. Syst. Technol.*, vol. 31, no. 1, pp. 425–438, Mar. 2021, doi: 10.1002/ima.22468.

[26] S. A. Mohammed, S. Darrab, S. A. Noaman, and G. Saake, "Analysis of breast cancer detection using different machine learning techniques," in *Data Mining and Big Data*. Singapore: Springer, 2020.

[27] X. Wang, I. Ahmad, D. Javeed, S. A. Zaidi, F. M. Alotaibi, M. E. Ghoneim, Y. I. Daradkeh, J. Asghar, and E. T. Eldin, "Intelligent hybrid deep learning model for breast cancer detection," *Electronics*, vol. 11, no. 17, p. 2767, Sep. 2022.

[28] K. D. S. Devi and C. S. Bindu, "CNN architectures to recognize handwritten Telugu characters," in *Proc. 4th Int. Conf. Smart Comput. Inform.*, vol. 1, Jul. 2021, pp. 225–239.


**L. LAKSHMI** received the M.Tech. degree from Jawaharlal Nehru Technological University Hyderabad, in 2012, and the Ph.D. degree from Jawaharlal Nehru Technological University Anantapur, Andhra Pradesh, in 2018. She is currently an Associate Professor with the Department of Data Science and AI, ICFAI University, Hyderabad, India. She has published more than 30 technical papers in various international journals, conferences, and book chapters. She holds eight patents. Her research interests include information retrieval systems, machine learning, deep learning, data science, and natural language processing.

**KUNADA DHANA SREE DEVI** received the M.Tech. and Ph.D. degrees from Jawaharlal Nehru Technological University Anantapur, Andhra Pradesh, in 2010 and 2016, respectively.

She is currently an Associate Professor with the Department of Computer Science and Engineering, GITAM University, Hyderabad, India. She has published more than 18 technical papers in various international journals, conferences, and book chapters. She is associated with many professional bodies, like CSI, ISTE, IAENG, and IEEE. Her research interests include machine learning, deep learning, natural language processing, data mining, database security, and network security.

**SHIKHA GUPTA** is currently a Professor with the Department of Computer Science and Engineering, University Institute of Engineering, Chandigarh University, Punjab. She is an academician and a researcher with extensive academic experience in prestigious institutes. She is leading the B.E. and M.E. courses in Computer Science (artificial intelligence and machine learning) with Chandigarh University. She has been teaching for the past 25 years and has supervised several M.Tech./Ph.D. students. She has several research articles published in SCI/Scopus journals and conferences. She has participated in and organized numerous FDPs, short-term courses, workshops, and seminars. Her research interests include artificial intelligence, blockchain technology, and machine learning.

**K. ADI NARAYANA REDDY** received the M.Sc. degree in mathematics from IIT Madras, in 2003, the M.Tech. degree in computer science from IIT Kharagpur, in 2008, and the Ph.D. degree from JNTU, Hyderabad, India, in 2015. In 2003, he was an Assistant Professor with SRK PG College. He is currently an Associate Professor with the Faculty of Science and Technology, ICFAI Foundation for Higher Education (IFHE). His research interests include machine learning, deep learning, and network security. He has 20 publications to his credit.

**SURESH KUMAR GRANDHI** received the B.Tech. degree in mechanical engineering from Nagarjuna University, Andhra Pradesh, India, in 1989, the M.E. degree in production engineering from Jadavpur University, Kolkata, in 1991, the Ph.D. degree from JNTU, Hyderabad, India in 2019, and the Diploma degree in AIML from the University of Hyderabad, in 2023. After his post-graduation, he continued his research as a Senior Research Assistant with the Production Engineering Department, Jadavpur University, till 1992. From 1992 to 2002, he worked in the manufacturing industry in different functional areas, including production, design, planning, and information technology in various capacities. In 2002, he was an Assistant Professor with the Faculty of Science and Technology, ICFAI Foundation for Higher Education (IFHE), where he is and an Associate Dean-Academics. His research interests include intelligent manufacturing, robotics, sustainable energy solutions, $CO_2$ capture, and the application of AI in mechanical engineering. He is the author of a book chapter, more than ten publications, and five inventions. He is a member of ISTE, ISHREA, and IEI. He was a recipient of the Government of India Fellowship for post-graduate studies.

**SANDEEP KUMAR PANDA** (Member, IEEE) is currently an Associate Professor and the Head of the Department of Artificial Intelligence and Data Science, Faculty of Science and Technology (IcfaiTech), ICFAI Foundation for Higher Education (Deemed to be University), Hyderabad, Telangana, India. He has 10, 00,000 seed money projects from IFHE. He has five edited books named *Bitcoin and Blockchain: History and Current Applications* (CRC Press, USA), *Blockchain Technology: Applications and Challenges* (Springer ISRL), *AI and ML in Business Management: Concepts, Challenges, and Case Studies* (CRC Press, USA), *The New Advanced Society: Artificial Intelligence and Industrial Internet of Things Paradigm* (Wiley Press, USA), and *Recent Advances in Blockchain Technology* (Springer ISRL), in his credit. He has published 50 papers in international journals and international conferences and book chapters in repute. He has 17 Indian patents on his credit. His research interests include blockchain technology, the Internet of Things, AI, and cloud computing. He is a member of ACM and a Life Member of IAENG. He received the 2020 Research and Innovation of the Year Award from the MSME, Government of India, and the DST, Government of India, New Delhi, in 2020. He received the Research Excellence Award from Brand Honchos, in 2022.